Underpotential Deposition of Cu on Boron-Doped Diamond Thin Films

F. Bouamrane,[†,‡] A. Tadjeddine,[‡] R. Tenne,[§] J. E. Butler,[⊥] R. Kalish,[∥] and C. Lévy-Clément*[,†]

LPSB, CNRS (UPR 1332), 1 Place Aristide Briand, 92195 Meudon, France; LURE, Bât. 209d, Université Paris-Sud (XI), 91405 Orsay, France; Department of Materials and Interfaces, Weizmann Institute, Rehovot 76100, Israel; Naval Research Laboratories, Washington, D.C. 20375-5000; and Solid State Institute, Technion, Haifa 32000, Israel

Received: May 5, 1997; In Final Form: August 29, 1997[⊗]

The deposition of copper on boron-doped diamond thin-film electrodes was investigated. Three kinds of boron-doped diamond films were studied: a film deposited on a silicon wafer, a second grown on a tungsten substrate, and a third, similar to the first, but surface-amorphized (bombarded) by ion beam irradiation. The films were investigated by a number of techniques. Linear potential sweep experiments in 0.1 M H_2SO_4 + 0.001 M $CuSO_4$ solution showed that, besides the peak due to bulk copper deposition, a "prewave" peak is present in the voltammogram of the first two electrodes and not in the third one. An electrochemical activation at negative potential was imperative for the appearance of the "prewave" peak. The amount of copper involved was less than 2% of a monolayer. The comparison between spectroscopic and electrochemical investigations leads to the interpretation that the "prewave" peak corresponds to an underpotential deposition of Cu on graphitic inclusions in the diamond electrode, or along the grain boundaries, probably by intercalation.

Introduction

The electrochemical properties of boron-doped diamond thin films have been under investigation lately.[1−8] Such electrodes have demonstrated very efficient reduction of nitrate (nitrite) into ammonia, and they can be polarized to large negative potentials without suffering damage.[4,5] Furthermore, these electrodes were shown to be dimensionally stable even in the most corrosive conditions, such as in fluoride solutions.[7] Added to that, both its hardness and its resistance against radiation damage make diamond film a very appropriate material for work under especially harsh environmental conditions, such as reduction of nuclear wastes (nitrate in basic solutions), electrowinning of metals from cyanide solutions for example, and high-temperature molten salt electrolysis. Electrodeposition of various metals (Au, Pt, Pb, and Hg) on diamond electrodes has been demonstrated.[6,7d] In the present work, copper deposition on diamond thin-film electrodes is investigated.

Experimental Section

Diamond thin films (A) were prepared by microwave-assisted chemical vapor deposition (μPCVD), using a methane-hydrogen mixture as a source gas. The films were rendered conductive by an in situ addition of borohydride gas at 10 ppm to the reactor chamber. The deposition was achieved on a Si(100) wafer (Sb doped with a resistivity of 0.01 Ω·cm) for the first type of film. The second type of film (B) used in this work was prepared by hot filament chemical vapor deposition (HFCVD), using tungsten substrate. Tables 1−3 summarize the details of film synthesis and their characteristics. Secondary ion mass spectrometry (SIMS) has shown that although the concentration of boron is only 10 ppm in the μPCVD reactor, the amount of boron incorporated into the film is very high (6×10^{20} cm^{-3}).[4b] SIMS analysis of HFCVD films (B)[9] shows that although the concentration of boron in the reactor is more than 2 orders of magnitude higher than in μPCVD, the amount of boron incorporated into the film is nearly the same ($>3 \times 10^{20}$ cm^{-3}). The carrier concentration is appreciably smaller for the HFCVD (vide infra), which indicates that not all the boron atoms incorporated into the film occupied substitutional sites. Although the conductivities of the films have not been established directly in this work, the films are expected to exhibit good conductivity. In fact, film A of this work is similar to film C (0.02 Ω·cm) used in ref 4b, while film B of this work was prepared by the same method and under similar conditions as film A in ref 4b (0.065 Ω·cm). Since electrode A was the subject of many electrochemical experiments prior to this work, it was necessary to study a fresh type A (μPCVD) diamond

TABLE 1: Summary of Synthesis of Diamond Films[a]

growth technique	μPCVD (A)	HFCVD (B)
filament		W
temp of filament (°C)		2200
filament−substrate distance (cm)		0.8
gas composition (%)	CH_4 (0.5),H_2 (99.5)	CH_4 (1), H_2 (99)
source of dopant (ppm)	B_2H_6 (10)	$B_2(C_2H_5)_3$ (2×10^3)
pressure (Torr)	40−50	50
gas flow rate (sccm)	100	100
temp of substrate (°C)	860	900
microwave power (W)	280−400	
frequency of microwave (GHz)	2.45	
substrate	Si(100), n-type (Sb), $\rho = 0.01$ Ω·cm	tungsten
estimated thickness (μm)	10	3.5

[a] HFCVD = hot filament chemical vapor deposition. μPCVD = microwave plasma chemical vapor deposition.

* To whom correspondence should be addressed.
[†] LPSB, CNRS (UPR 1332).
[‡] LURE.
[§] Weizmann Institute.
[⊥] Naval Research Laboratories.
[∥] Solid State Institute, Technion.
[⊗] Abstract published in *Advance ACS Abstracts,* December 15, 1997.

S1089-5647(97)01516-2 CCC: $15.00
Published on Web 01/01/1998

TABLE 2: Summary of SEM Characterization

film	crystallinity	grain size (μm) (statistical weight)		texture	remarks
A	polycrystalline	3−7 (90%)	1−2 (10%)	(111)	irregular surface morphology
B	polycrystalline	1.5−3 (80%)	0.8−1.2 (20%)	(111) and (100)	grain with regular geometry

TABLE 3: Summary of Characterization of Film Texture with a Profilometer

	maximal roughness (μm)		minimal roughness (μm)	
film	width	height	width	height
A	4−9	0.3−0.5	1−4	0.1−0.3
B	2−4	0.1−0.3	0.3−2	0.03−0.1

film without any prior electrochemical history, which is termed sample C. Similar electrochemical experiments were undertaken with a fresh diamond film (μPCVD) whose surface was bombarded for 10 min with Ar^+ ions (4 kV current intensity of 30 μA with a base pressure of 2×10^{-6} Torr) (sample D).

The electrical contact to the diamond film was established, through the conductive substrate, on the backside of A electrodes by first scratching the Si surface and then rubbing it with an In−Ga alloy. All samples were fixed to a Cu wire with a silver paste. The electrodes were insulated, except for the front diamond surface using a silicon rubber (Dow Corning 3145 RTV). The samples A, C, and D (diamond films deposited on silicon substrate) were cleaned first by immersion in a hot nitric acid for 10 min to remove metallic impurities and subsequently rinsed thoroughly with ultrapure water, whereas for the sample B (diamond film deposited on tungsten substrate) the cleaning procedure was slightly modified by an immersion in a hot concentrated sulfuric acid for 10 min instead of hot nitric acid in which tungsten corrodes. Finally, all samples were immersed for 10 min in ultrapure boiling water. Electrodes A and B experienced many electrochemical cycles in the negative potential range down to −2 V, before being used for copper deposition experiments.

Electrochemical measurements were performed in a glass cell. Ar gas was bubbled through the solution in order to remove oxygen. A Pt foil was used as counter electrode, and the reference electrode was a saturated calomel electrode (SCE). All the potentials in this work are reported relative to this electrode. Electrochemistry was performed first in a 0.1 M H_2SO_4 and then in a 0.1 M H_2SO_4 + 0.001 M $CuSO_4$ solutions. H_2SO_4 and $CuSO_4$ solutions were prepared from high-purity chemicals (Aldrich) and ultrapure water (18 MΩ·cm).

Raman spectra were measured, with standard setups, in the laboratories from which the films originated. A JEOL Model 840 scanning electron microscope (SEM) was used for imaging of the film surface. A X-ray energy dispersive (EDS) analyzer Leica stereo scan 440 Model equipped with a Si−Li diode was used for the chemical analysis of the film surface during the various stages of the processes. X-ray absorption near edge spectroscopy (XANES) was performed on the SA72 beam line, monochromatized by a 10 m toroidal gratings, at the SuperAco storage ring at LURE (Orsay). The XANES and X-ray photoelectron spectroscopy (XPS) measurements were performed in a UHV analysis chamber (base pressure 10^{-11} Torr). A reaction chamber for Ar^+ bombardment was connected to the analysis chamber. The XANES was measured by recording the partial electron yield mode (PEY) between 278 and 380 eV with a resolution of 0.2 eV. For the XPS measurements, the Mg Kα (1253.6 eV) line with a full width at half-maximum (fwhm) of 0.8 eV, a hemispherical mirror electron analyzer (CLAM2), and a channeltron detector of VG Instruments (all present in the analyzer chamber) were used. The spectra were collected in the analyzer constant energy mode, with a pass energy of 50 eV. The analyzer resolution is approximately 0.2 eV. The C 1s and Si 2p spectra were acquired with a 0.1 eV/step energy interval. Fourier transform infrared absorption (FTIR) measurements, which are mentioned only briefly in this work and will be published elsewhere,[10] were measured with a DA8 Bomem system with glowar source, KBr beam splitter, and MCT detector, between 700 and 5000 cm^{-1} with a resolution of 4 cm^{-1}. One spectrum was the average of 200 scans. The surface roughness of the films was determined by a Tencor Model p1 profilometer.

TABLE 4: Analysis of the C 1s XPS Peak (Resolution 0.2 eV)

sample	peak position (eV)	fwhm (eV)
B	283.5	1.4
A	283.4	1.3
D	283.3	2.2

Results

1. Characterization. The Raman spectra of both films (electrodes A and B) consisted of an intense narrow peak at 1332 cm^{-1} which is assigned to crystalline sp^3-hybridized carbon. Whereas the Raman spectrum of sample A was published before,[5] that of sample B shown in Figure 1 is indicative of a good-quality diamond film. The additional wide Raman response around 1500 cm^{-1} indicates the presence of sp^2 carbon in a very small amount (maybe a few percent). The morphology of the films was examined by SEM (Figure 2). The results are also summarized in Table 2. The surfaces of all samples appear to be very uniform with grain size in general varying between 3 and 7 μm for electrode A. The crystallites appear to be mostly (111) oriented in the case of sample A, whereas both (111) and to a lesser extent (100) faces are present in film B. The grain size for electrode B was mainly between 1.5 and 3 μm, and the coverage of the W substrate by the diamond film is also uniform. The morphology of sample D has not changed vis-à-vis sample A (C), which indicates that only the sample surface was influenced by the irradiation. EDS analysis of the sample surfaces did not show traces of uncovered

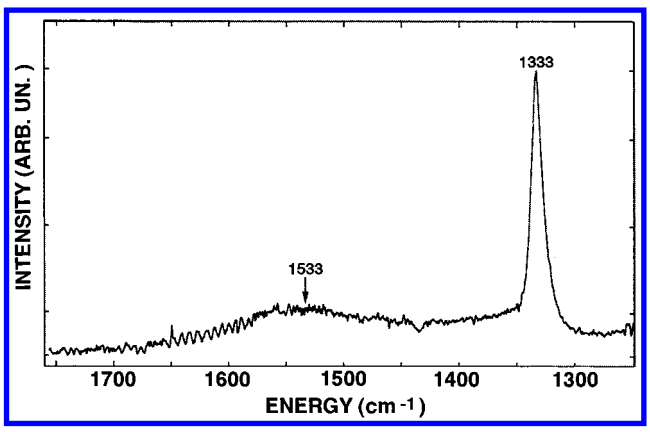

Figure 1. Raman spectrum of boron-doped diamond film (sample B).

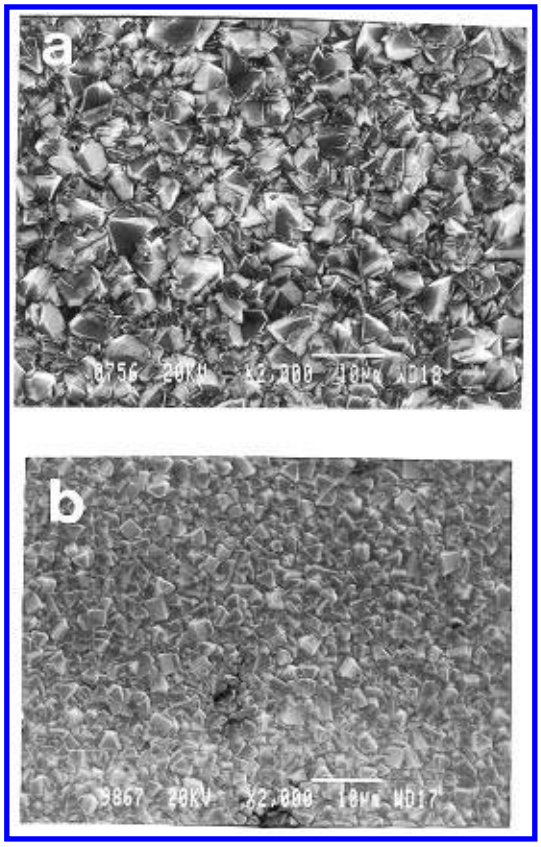

Figure 2. SEM micrographs of diamond films A and B.

surface, which could make the Si (or W) substrate susceptible to corrosion due to electrochemical processes with the solution.

Detailed infrared (IR) characterization of the films was carried out and will be published elsewhere.[10] The IR absorption mode at 1280 cm^{-1} is suggestive of the quality of the substitutional doping of the diamond lattice by boron.[11] In brief, the symmetry-forbidden IR transition of diamond is alleviated by the presence of boron dopant atoms in substitutional sites, which remove the inversion symmetry of the lattice near the dopant atom. Sample A, which was manufactured by μPCVD, shows a distinct IR absorption between 1260 and 1330 cm^{-1}. This method was shown before to be very efficient for boron doping of diamond.[4b] On the contrary, sample B, which was synthesized by HFCVD, is transparent in the entire range (500−5000 cm^{-1}). Indeed, the latter technique was shown to be less effective for boron doping than the previous method.[4b] It is not clear at this point which sites are occupied by the boron atoms, in addition to the substitutional sites of the lattice.

The surface roughness was studied by profilometry in order to obtain a quantitative estimation of the effective working surface area of the electrodes.[10] The corrected (effective) surface area of the electrodes was 0.34 cm^2 for sample A, which corresponds to an increase of 20% with respect to the geometrical surface area, and 0.63 cm^2 (15% increase) for sample B. The corrected surface area of samples C and D were 0.2 and 0.42 cm^2, respectively.

XPS analysis of the films, cleaned by the procedure described above, shows that oxygen is omnipresent in all films. The electrochemical experiments increase the amount of oxygen present on the diamond surface. The Si 2p peak can be assigned to SiO_2 (102.7 eV).[12] The height of the Si peak increases 2−3-fold after ion bombardment (D). These sources of contamination could be ascribed either to some reaction of the reactor chamber with the methane−hydrogen plasma during the synthesis of the films or to the insulating silicon rubber used for the sealing of the electrode and to the conductive lacquer which was used to affix the electrode to the Cu wire. The source of this contamination is discussed below. Sample B was found to contain a small quantity of nitrogen, which is likely to come from the gas source used for the synthesis. Figure 3 shows a closeup of the C 1s spectra of three samples (A, B, and D). The maximum of the XPS peaks is similar for the three samples; however, a distinguishable broadening of the peak from 1.3 to 2.2 eV is obtained after bombardment of the diamond surface (D) (Table 4). This broadening can be attributed to the amorphization of the bombarded diamond surface. The C 1s peak of the three samples could be deconvoluated in one principal peak corresponding to a C−C bond (relative intensities are 79%, 78%, and 87% for samples A, B, and D, respectively) and one or two small satellite peaks at the higher energies attributed to C-hydrocarbon (with relative intensities of 16.5%, 22%, and 8% for samples A, B, and D, respectively) and C−O bonds (4.5% and 5% for samples A and D, respectively). Among all the impurities detected by XPS, the only impurity whose concentration decreased after Ar^+ bombardment was the hydrogenated carbon.

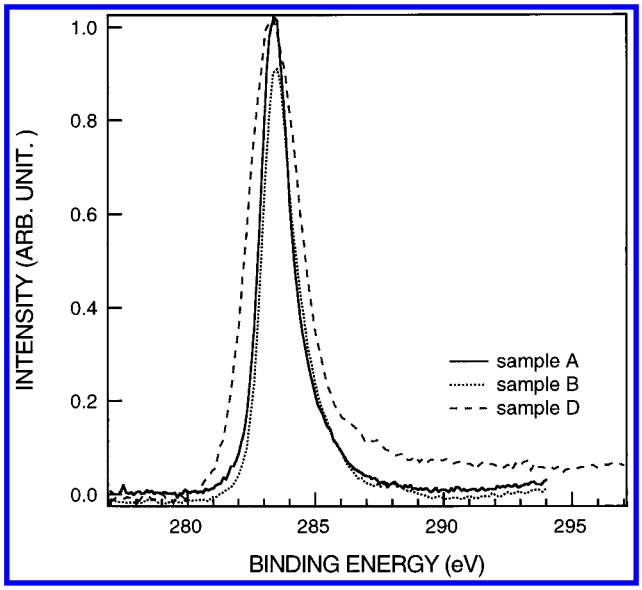

Figure 3. XPS spectra of the C 1s region of samples A, B, and C.

The XANES spectra of the films (cleaned with the acidic procedure) are shown in Figure 4. The spectra of samples A and B, showing a modulated structure (with absorptions situated at 292.4, 298, and 305 eV) after the main absorption edge at 288.6 eV (sp^3 carbon hybridized), are very similar to the spectra of single-crystal diamond[13] and to previously studied diamond thin films.[14] Most importantly, the 1s π^* transition (285.4 eV peak), which is associated with unsaturated carbon dangling bonds, is rather small in the two films. On the contrary, the XANES measurement of sample D indicates that the surface of the film became amorphous[15] (Figure 4). A very strong absorption at 285.4 eV, which indicates the abundance of unsaturated carbon atoms at the film surface, is observed. Furthermore, the four or more distinct peaks at 290−310 eV coalesce in this sample into a single very broad peak, which indicates a substantial amount of disorder in the lattice of the diamond surface. The presence of the 1s π^* transition in sample A which was submitted to a 10 min concentrated hot HNO_3 treatment shows that this pretreatment does not remove all the residual graphitic carbon impurities. Indeed, to remove the

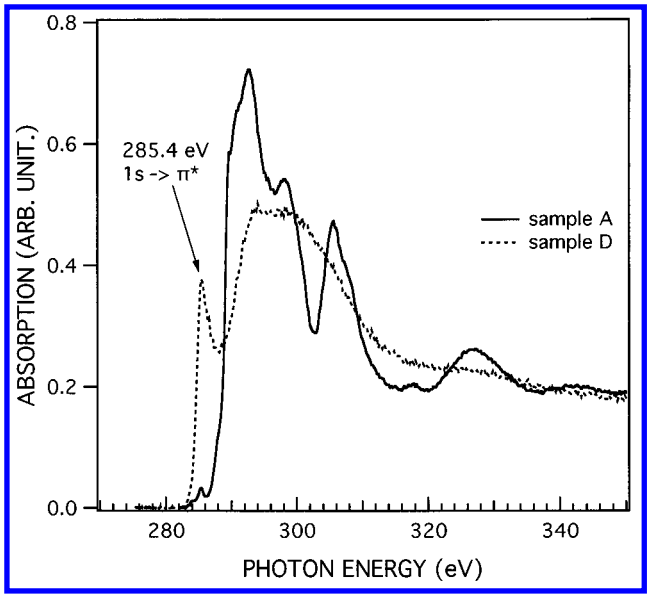

Figure 4. C K-shell XANES spectra of samples A and D.

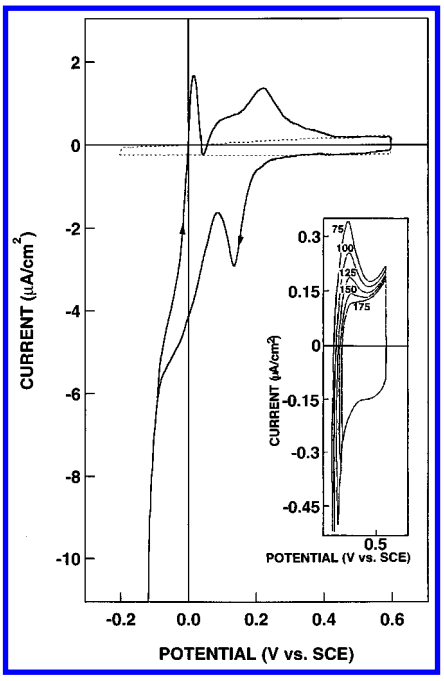

Figure 5. Cyclic voltammograms of electrode A. The electrode surface area, estimated from roughness measurement, is 0.34 cm^2: (---) 0.1 M H_2SO_4 solution, (—) 0.1 M H_2SO_4 + 0.001 M $CuSO_4$ solution. The scan rate is 50 mV/s. In the inset are shown the $I-V$ curves of the same electrode with E_i = 600 mV and E_f varying as indicated on each curve.

graphitic impurities stronger oxidant acids are used such like sulfochromic acid.[16]

2. Voltammogram in Acid Solution. Diamond electrodes A, B, and C gave a very broad potential range over which no significant water decomposition occurred in both neutral (0.1 M KCl) and basic (1 M NaOH) electrolytes, in agreement with claims[5−8] in the literature.

Cyclic voltammetry in Cu^{2+}-free supporting electrolyte (0.1 M H_2SO_4) was performed and is shown in Figure 5 for sample A and in Figure 6 for sample B (dashed line). The voltammograms are flat throughout the potential range from an initial potential E_i = 600 mV to a final potential E_f = −300 mV, which is a characteristic of the charging of the double-layer region. The capacitance values at 0 V are 2.0 $\mu F/cm^2$ for film A and 4.5 $\mu F/cm^2$ for film B, in very good agreement with values published for diamond thin films which were deposited on silicon[7] but an order of magnitude lower or larger than the values published in refs 1 and 8, respectively. Consequently, these curves could serve later as a baseline for quantitative evaluation of the charge used for copper deposition from copper-containing solutions. This is done by estimating the area of a reduction peak between two given potentials, in a copper-containing solution, and subtracting the charge of the double-layer region taken from the measurement in a 0.1 M H_2SO_4 solution alone.

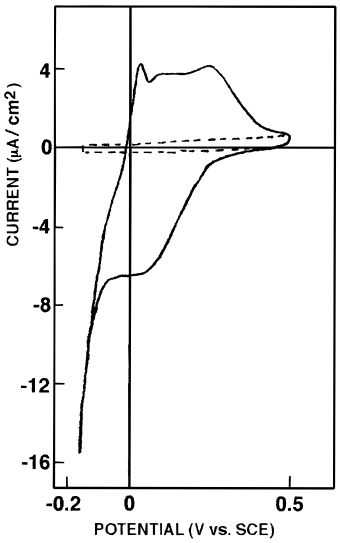

Figure 6. Cyclic voltammograms of electrode B. The surface of the electrode, which was estimated from roughness measurement, is 0.63 cm^2: (---) 0.1 M H_2SO_4 solution, (—) 0.1 M H_2SO_4 + 0.001 M $CuSO_4$ solution. The scan rate is 50 mV/s.

3. Copper Deposition. *3.1. Electrode A. a. Voltammogram.* A cyclic voltammogram of electrode A performed in 0.1 M H_2SO_4 + 0.001 M $CuSO_4$ solution, with E_i = 600 mV and E_f = −150 mV, shows the presence of several structures that are related to the electrochemistry of copper ions (Figure 5). Between 600 and 300 mV the voltammogram is flat and is identical with the one obtained in 0.1 M H_2SO_4. A reduction peak centered at 125 mV is noticed. From 80 mV the current starts to increase, with a strong rise below −100 mV. During the sweep in the reverse direction, two oxidation peaks are observed. The narrow peak centered at 10 mV has a small intensity. The second peak between 80 and 450 mV can be decomposed into two contributions, the largest one being centered at 210 mV whereas the second one corresponds to a shoulder situated at 100 mV. The standard potential of the Cu/Cu^{2+} couple being equal to 0.094 V vs SCE,[17] the Nernst potential for a Cu^{2+} concentration of 10^{-3} M is equal to 0.005 V vs SCE. The increase of the cathodic current around 0 V can be attributed to the bulk copper deposition and the narrow oxidation peak at 10 mV to the oxidation of the bulk deposited copper. At potentials less than −100 mV, the current increase is due to the onset of water reduction on the deposited copper. The reduction peak centered at 125 mV appears at a higher potential than the reversible Nernst potential and is named the "prewave" peak. To understand the origin of the "prewave" peak, complementary experiments have been accomplished such as cyclic voltammetry with stepwise negative increasing potential limits, influence of the variation in the sweep rate, and the duration of the polarization at E_f = −150 mV on the intensity and position of the "prewave" and oxidation peaks.

b. Cyclic Voltammetry with Increasing Stepwise Negative Potential Limits. Starting from 600 mV, a series of voltammograms with increasing stepwise negative limits up to $E_f = -150$ mV have been carried out using potential steps of 10−25 mV (inset of Figure 5). This series of measurements shows that the "prewave" peak at 125 mV and the oxidation peak at 210 mV are associated with each other. Their intensities increase gradually with the decrease of the potential until E_f reaches −100 mV where they stabilize to a maximum value. The intensity of the oxidation peak at 100 mV varies in a similar way, with the decrease of E_f. No reduction peak associated with this oxidation peak was observed, most probably because it is hidden by the strong cathodic current which appears at 80 mV, due to its weak intensity. The oxidation peak at 10 mV (which appears when E_f reaches −100 mV) shows a very different behavior as its intensity increases without being saturated when E_f decreases.

c. Effect of Varying the Scanning Speed. The effect of varying the scanning speed on the deposition and stripping reactions was investigated. Voltammograms were taken from $E_i = 600$ mV to $E_f = -140$ mV with speeds of 10, 20, 50, and 100 mV/s. When the speed increased from 10 to 100 mV/s, the maximum of the 125 mV "prewave" peak shifted by ca. 30 mV, cathodically. The corresponding charge for the "prewave" peak remained unaltered for all speeds, fluctuating between 4.1 and 5.3 μC/cm^2 for the deposition (between 90 and 300 mV) and between 5.3 and 6.2 μC/cm^2 for the oxidation peaks (between 50 and 500 mV). This corresponds to the coverage of a small fraction of the surface (about 1% of a monolayer). On the contrary, the charge passed during the deposition and stripping of bulk Cu increased when the scan speed decreased, since the amount of deposited Cu increases when the scan speed is decreased.

d. Effect of the Duration of the Polarization at $E_f = -140$ mV. In another experiment, the scan, which started at $E_i = 600$ mV, was interrupted at $E_f = -140$ mV for various delay times. Afterward, the potential scan was resumed in the anodic (stripping) direction ($E_f \rightarrow E_i$). The delay times used were 0, 1, and 2 s. No influence of the delay times on the oxidation peaks was detected (Figure 7), while a drastic increase of the stripping peak (centered between 10 and 40 mV) of bulk Cu was observed as the delay time increased, since more metal has been deposited in this case.

e. Interpretation. Several observations favor the interpretation that a copper under potential deposition (UPD) phenomenon occurs on electrode A: (i) the position of the "prewave" reduction peak at 125 mV which is more positive than the Nernst potential; (ii) the reversibility of the phenomenon—the deposition and the oxidation occur at 125 mV and 210 mV, respectively; (iii) the saturation of the intensity of the two peaks when the potential reaches a certain E_f value (−100 mV), which means that the amount of charge involved is limited; (iv) the sweeping rate showing no influence on the amount of charge involved; (v) the delay times having no influence on the UPD oxidation peaks. However, the very low coverage of the surface, about 1% of a monolayer, leads us to believe that the phenomenon does not take place on diamond material, but rather on its defects such as graphite or on surface impurities. Though the phenomenon is not truly an UPD on diamond, we will keep for convenience in the text the term "Cu-UPD" to designate the "prewave" peak and the corresponding oxidation peak. The large cathodic current and the oxidation peak at 10−40 mV correspond to the deposition and stripping of bulk Cu film, respectively. The small oxidation peak at 100 mV can be ascribed to the stripping of the second monolayer of Cu UPD or corresponds to a second stripping peak of the first monolayer as seen with UPD of copper on Pt.[18]

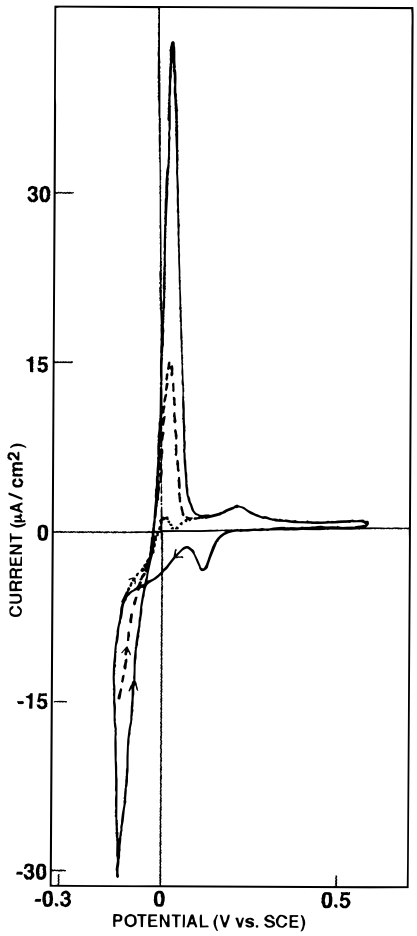

Figure 7. Cyclic voltammograms of electrode A in 0.1 M H_2SO_4 + 0.001 M $CuSO_4$ solution. Effect of polarization time at −142 mV: (•••) 0, (---) 1, and (—) 2 s.

3.2. Electrode B. The results for Cu deposition on diamond thin film grown on tungsten (sample B) are shown in Figure 6. The voltammograms were determined between $E_i = 500$ and $E_f = -175$ mV. Here also a "prewave" reduction peak is present which appears as a shoulder on the bulk Cu deposition current curve. The corresponding oxidation peak is observed at 250 mV with a shoulder at 100 mV. When E_f reaches −140 mV, an oxidation peak corresponding to the stripping of bulk deposited copper appears around 40 mV. The height of the stripping peak increases as E_f goes to more negative potential values. It is therefore concluded that the oxidation of the Cu-UPD in sample B occurs at a potential that is shifted by approximately 30 mV anodically, compared with that of sample A. No Cu islands could be observed by SEM on samples A and B after Cu-UPD. The fact that no EDS Cu signal was obtained suggests that the Cu is deposited uniformly and in very small quantities, below the detection limit of the EDS (approximately 0.1%) at this potential range.

3.3. Electrode C. To further investigate the Cu-UPD phenomenon, similar experiments were conducted with a fresh diamond film on silicon (sample C), which is similar to electrode A, but was not previously used in any electrochemical experiment. The working surface for this electrode was 0.2 cm^2. First measurements were made in the supporting electrolyte (0.1 M H_2SO_4 solution) between $E_i = 600$ mV and $E_f = -200$ mV (Figure 8a). From this voltammogram, the double-layer ca-

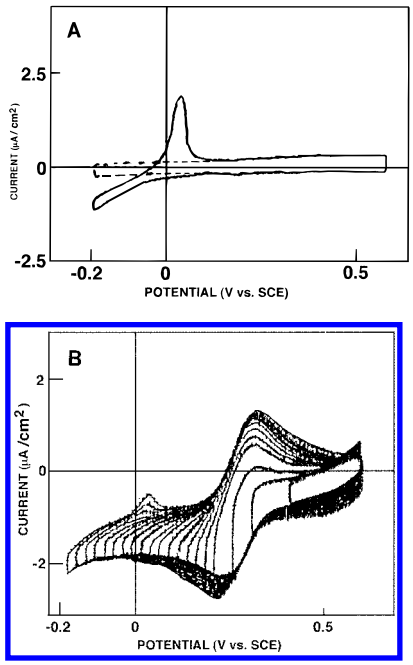

Figure 8. Cyclic voltammograms of electrode C. Estimated electrode surface is 0.2 cm^2. Scan rate is 50 mV/s. (a) Before electrochemical activation: (---) 0.1 M H_2SO_4 solution, (—) 0.1 M H_2SO_4 + 0.001 M $CuSO_4$ solution; (b) After electrochemical activation at −2 V for a few seconds, 0.001 M $CuSO_4$ solution.

pacitance was calculated as 3.5 μF/cm^2, a value with the same order of magnitude as films A and B.

In the next step, cyclic voltammetry was performed in a 0.1 M H_2SO_4 + 0.001 M $CuSO_4$ solution starting with E_i = 600 mV and gradually decreasing the final potential E_f from 400 mV down to −200 mV in 25 mV steps (Figure 8a shows only one curve with E_f = −200 mV). Here, no sign of Cu-UPD was detected. Only bulk deposition and stripping of copper were detected (stripping peak at 40 mV). The electrode seemed to be passivated at the beginning of the negative potential scan, and it was necessary to reach larger negative potentials before any electrochemical reaction was evident. For this reason an electrochemical activation step was undertaken by polarizing the electrode for a few seconds at −2 V without removing it from the solution (hydrogen evolution could be discerned). Afterward, the electrode was cycled between E_i = 400 mV and E_f = 600 mV for a few minutes in order to remove any copper deposited during the cathodic polarization step. Subsequently, cyclic voltammetry of electrode C exhibited clear underpotential phenomena (see Figure 8b). As soon as E_f was less than 300 mV, a reduction current started, which increased as E_f was moved further in the cathodic direction. In parallel to that, an oxidation feature appeared once E_f was less than 250 mV and grew larger as E_f decreased further. The UPD peak position was found to be at 235 mV and the stripping UPD peak position at 330 mV, which represents a +120 mV shift in the UPD peak as compared to electrode A and about +80 mV when compared to electrode B.

When E_f reached −150 mV, a second oxidation peak appeared at 40 mV, which corresponds to the stripping of bulk copper. No evolution in the UPD peaks was noticeable after E_f reached about −150 mV, while the bulk deposition and stripping features varied appreciably with E_f (Figure 8b). The charge for the UPD peaks was 7.1 ± 0.3 μC/cm^2 for the cathodic peak and 8.4 ± 0.4 μC/cm^2 for the stripping peak. This charge corresponds to less than 2% of a monolayer, i.e., the same order as that of electrodes A and B. The effect of the scanning speed and the effect of the delay time at E_f were elucidated; the results showed no noticeable difference with respect to the previous electrodes (A and B). The main conclusion from this experiment is that the electrochemical treatment imposed on this electrode (C) activated some specific sites on the electrode, which permitted underpotential deposition of copper.

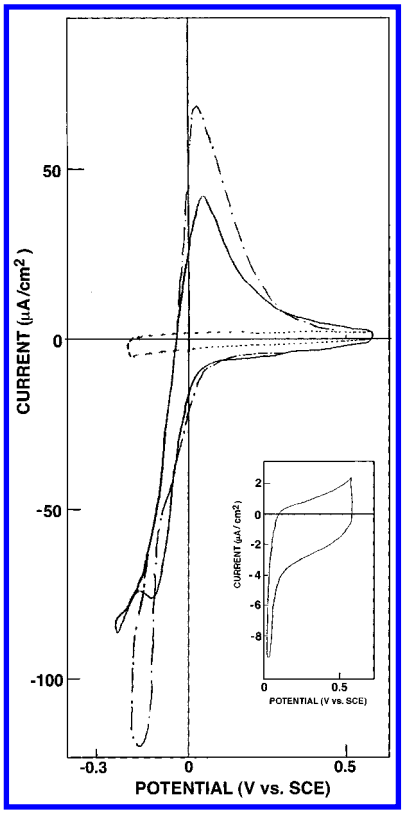

Figure 9. Cyclic voltammograms of diamond doped thin film on silicon which was bombarded for 10 min with Ar^+ (electrode D) in (---) 0.1 M H_2SO_4 solution and (—) 0.1 M H_2SO_4 + 0.001 M $CuSO_4$ solution before electrochemical activation; and in (−·−) 0.1 M H_2SO_4 + 0.001 M $CuSO_4$ solution after being activated for a few seconds at −2 V. Effective electrode surface is 0.42 cm^2, scan rate is 50 mV/s. Inset: cyclic voltammogram between 600 and 0 V of electrode D after electrochemical activation at −2 V for a few seconds. The solution is 0.1 M H_2SO_4 + 0.001 M $CuSO_4$. Scan rate is 50 mV/s.

3.4. Electrode D. Electrode D went through exactly the same preparation procedure as the previous electrode (C), and the same electrochemical experiments were carried out as for the other three electrodes. The voltammogram performed between 600 and −200 mV in a H_2SO_4 solution shows that the double-layer capacitance (80−100 μF/cm^2) is 30−50 time larger than for the electrodes A and C. The bombardment not only amorphized the surface of the diamond electrode but also increased the reactional surface by a factor of 30−50. As can be seen from Figure 9, no underpotential deposition was taking place with this electrode (full line). Activation of the electrode at −2 V during a few seconds did not lead to UPD features, as can be seen in the inset of Figure 9 (here the potential range varies between E_i = 600 mV and E_f = 0 mV). For an E_f less than −200 mV, bulk deposition and stripping features, similar to the previously obtained voltammograms, were observed (Figure 9). These measurements show that no Cu-UPD takes place on the new electrochemically active sites created by Ar^+ bombardment. However, we cannot totally rule out the presence of a Cu-UPD phenomenon on diamond defects (graphitic impurities) similar to that observed on the other electrodes, because its contribution would be hidden in the capacitive current.

Discussion

Direct correlation between underpotential deposition of copper and the presence of impurities detected by XPS such as Si and oxidized or hydrogenated carbon is not straightforward.

Cu-UPD on other forms of carbon than diamond has already been observed. It was performed in ref 19 on pyrolytic graphite using 0.1 M $KClO_4$ + 0.1 M $HClO_4$ + 5×10^{-5} M $Cu(NO_3)_2$. The main UPD stripping peak was at 150 mV (vs SCE) which represented one monolayer of copper on the electrode. A second UPD stripping peak was observed at 350 mV. In ref 20 the UPD of copper on stress-annealed pyrolitic graphite was not seen (the solution used was 0.5 M Na_2SO_4 + 5×10^{-4} M $CuSO_4$), while it could be observed for other metal ions, specifically Hg^{2+}, Pb^{2+}, and Li^+. It is therefore not unlikely that the sites for Cu-UPD on the diamond electrode are linked to residual sp^2 carbon, which cannot be completely avoided. The most favorable site for Cu-UPD deposition would appear to be the van der Waals (vdW) gap between two graphite planes, i.e., Cu intercalation. The intercalation takes place most easily when the graphite crystallites are oriented with their (1120) prismatic faces toward the solution. However, in most studies the graphite electrodes are placed with their basal (0002) face oriented toward the solution, and the intercalation takes place through grain boundaries and monatomic steps (surface edge dislocations) on the basal plane. Furthermore, it is not uncommon that impurities and solvent molecules adhere to the (1120) face and block the access for the vdW gap to intercalated atoms. Therefore, some activation process is required before Cu intercalation (UPD) takes place. This also may explain the discrepancies between the Cu-UPD results of the various electrodes. The fact that the amorphized surface of sample D may not accommodate Cu-UPD is not surprising, since the energy of the impinging Ar^+ ions damages not only the diamond lattice but also the graphitic nanocrystallites that are left in the diamond matrix near the surface, and are presumably responsible for the Cu-UPD. It will be necessary to study this phenomenon in greater detail in order to obtain a more conclusive understanding of the Cu-UPD mechanism in carbonaceous electrodes and diamond electrodes in particular.

Conclusions

A "prewave" peak situated at a potential more positive than the peak for the deposition of bulk copper is observed in the linear potential sweep experiments on diamond electrodes in copper-containing acidic solutions. The investigations suggest that it is associated with the underpotential deposition (or intercalation) of copper on crystalline defects in the diamond thin films, probably graphitic inclusions. The amount of Cu involved is very small (about 1−2% of a monolayer). There is evidence that the electrochemical activation of the diamond electrode activates the surface, rendering underpotential deposition of Cu on the diamond defects possible. Further work is needed to understand which type of site is responsible for this phenomenon. This kind of study could be of a great interest for future applications of diamond thin films in both electrochemistry and electronics.

Acknowledgment. The authors are grateful to Carine Laffon and Philippe Parent for the XANES and XPS measurements. This work was supported by a grant from the European Community (Contract C11*-CT93-0065). We acknowledge the Ministère des Affaires Etrangères (France) and the Israeli Ministry of Science and Arts for the support through an Arc en Ciel (Keshet) project.

References and Notes

(1) Pleskov, Y.; Sakharova, A.; Krotova, M. D.; Bouilov, L. L.; Spitsyn, B. V. *J. Electroanal. Chem*. **1987,** *228*, 19.

(2) (a) Sakharova, A. Y.; Sevast'yanov, A. E.; Pleskov, Y. V.; Templitskaya, G. L.; Surikov, V. V.; Voloshin, A. A. *Electrokhimya* **1991**, *27*, 239. (b) Sakharova, A. Y.; Nyikos, L.; Pleskov, Y. V. *Electrochim. Acta* **1992**, *37*, 973. (c) Sakharova, A. Y.; Pleskov, Y. V.; Di Quatro, F.; Piazza, S.; Sunseri, C.; Teremetskaya, I. G.; Varnin, V. P. *J. Electrochem. Soc*., **1995**, *142*, 2704.

(3) Patel, K.; Hashimoto, K.; Fujishima, A. *Denki Kagaku* **1992**, *60*, 659.

(4) (a) Tenne, R.; Patel, K.; Hashimoto, K.; Fujishima, A. *J. Electroanal. Chem*. **1993**, *347*, 409. (b) Reuben, C.; Galun, E.; Cohen, H.; Tenne, R.; Kalish, R.; Muraki, Y.; Hashimoto, K.; Fujishima, A.; Butler, J. E.; Lévy-Clément, C. *J. Electroanal. Chem*. **1995**, *396*, 233.

(5) Bouamrane, F.; Tadjeddine, A.; Butler, J. E.; Tenne, R.; Lévy-Clément, C. *J. Electroanal. Chem*. **1996**, *405*, 95.

(6) (a) Miller, B.; Kalish, R.; Feldman, L. C.; Katz, A.; Moriya, N.; Short, K.; White, A. E. *J. Electrochem. Soc.* **1994**, *141*, L41. (b) Vinokur, N.; Miller, B.; Avyigal, Y.; Kalish, R. *J. Electrochem. Soc*. **1996**, *143*, L238.

(7) (a) Swain, G. M.; Ramesham, R. *Anal. Chem*. **1993**, *65*, 345. (b) Swain, G. M. *Adv. Mater*. **1994**, *6*, 388. (c) Swain, G. M. *J. Electrochem. Soc*. **1994**, *141*, 3382. (d) Awada, M.; Strojek, J. W.; Swain, G. M. *J. Electrochem. Soc*. **1996**, *142*, L42. (e) DeClements, R.; Swain, G. *J. Electrochem. Soc*. **1997**, *144*, 856.

(8) Martin, H. B.; Argoitia, A.; Landau, U.; Anderson, A. B.; Angus, J. C. *J. Electrochem. Soc*. **1996**, *143*, L133.

(9) Kalish, R. Personal communication.

(10) Bouamrane, F. Ph.D. Thesis, University of Paris XI, Orsay, 1997. Bouamrane, F.; Parent, P.; Laffont, C.; Tadjeddine, A.; Lévy-Clément, C. To be published.

(11) Walker, J. *Rep. Prog. Phys.* **1979**, *42*, 108.

(12) (a) Belton, D. N.; Harris, S. J.; Schmeig, S. J.; Weiner, A. M.; Perry, T. A. *Appl. Phys. Lett*. **1989**, *54*, 416. (b) Arezzo, F.; Severini, E.; Zacchetti, N. *Surf. Interface Anal*. **1994**, *22*, 218.

(13) (a) Morar, J. F.; Himpsel, F. J.; Hollinger, G.; Hugues, G.; Jordan, J. L. *Phys. Rev. Lett*. **1985**, *54*, 1960. (b) Nithianandam, B. J. *Phys. Rev. Lett.* **1992**, *269*, 3108.

(14) (a) Takata, Y.; Edamatsu, K.; Yokoyama, T.; Seki, K.; Tohnan, M.; Okada, T. *Jpn. J. Appl. Phys*. **1989**, *28*, L1282. (b) Capehart, T. W.; Perry, T. A.; Beetz, C. B.; Belton, D. N.; Fischer, G. B.; Beall, C. E.; Yates, B. N.; Taylor, J. W. *Appl. Phys. Lett.* **1989**, *55*, 10.

(15) (a) Fink, J.; Muller-Heinzerling, T.; Pfluger, J.; Bubenzer, A.; Koidl, P.; Crecelius, G. *Solid State Commun.* **1983**, *47*, 687. (b) Comelli, G.; Stohr, J.; Robinson, C. J.; Jark, W. *Phys. Rev. B* **1988**, *38*, 7511.

(16) Grot, S. A.; Gildenblat, G. S.; Hatfield, C. W.; Wronski, C. R.; Badzian, A. R.; Badzian, T.; Messier, R. *IEEE Electron Dev. Lett.* **1990**, *11*, 100.

(17) *Handbook of Chemistry and Physics*; CRC Press: Boca Raton, FL, 1988−1989; p 152.

(18) Kolb, D. M. In *Advances in Electrochemistry and Electrochemical Engineering*; Gerischer, H., Tobias, C. W., Eds.; Wiley: New York, 1978; Vol. 11, p 125.

(19) Vassos, B. H.; Mark, H. B., Jr. *J. Electroanal. Chem*. **1967**, *13*, 1.

(20) Morcos, I. *J. Electroanal. Chem*. **1975**, *66*, 250.